# Electrostatic Layer-by-Layer Assembly of CdSe Nanorod/Polymer Nanocomposite Thin Films

Sean A. McClure,[†,‡] Brian J. Worfolk,[†,‡] David A. Rider,[†] Ryan T. Tucker,[§] Jordan A. M. Fordyce,[†] Michael D. Fleischauer,[‡] Ken D. Harris,[‡] Michael J. Brett,[‡,§,*] and Jillian M. Buriak[‡,†,*]

National Institute for Nanotechnology, National Research Council Canada, 11421 Saskatchewan Drive, Edmonton, Alberta, Canada T6G 2M9, Department of Chemistry, University of Alberta, Edmonton, Alberta, Canada T6G 2G2, and Department of Electrical and Computer Engineering, University of Alberta, Edmonton, Alberta, Canada T6G 2V4

**ABSTRACT** Electrostatic layer-by-layer assembly was the basis for the synthesis of multilayer nanorod/polymer composite films. Cationic and water-soluble CdSe nanorods (NRs) were synthesized and partnered with anionic polymers including poly(sodium 4-styrenesulfonate) (PSS) and two polythiophene-based photoactive polymers, sodium poly[2-(3-thienyl)-ethoxy-4-butylsulfonate (PTEBS) and poly[3-(potassium-6-hexanoate)thiophene-2,5-diyl] (P3KHT). Controlled multilayer growth is shown through UV−vis spectroscopy, cross-sectional SEM and surface analytical techniques including atomic force microscopy. The formation of an intimate nanorod/conducting polymer bulk heterojunction is confirmed through cross-sectional SEM, TEM, and scanning Auger analysis. A series of photovoltaic devices was fabricated on ITO electrodes using CdSe NRs in combination with PTEBS or P3KHT. A thorough device analysis showed that performance was limited by low short circuit current although charge transfer was confirmed in the ELBL nanocomposite thin films.

**KEYWORDS:** water-soluble CdSe nanorods • ligand exchange • polythiophene • layer-by-layer • multilayer thin films • charge transfer

## INTRODUCTION

Layer-by-layer (LBL) assembly has attracted a great deal of attention in recent years as a facile method for creating nanocomposite thin films with a high degree of control (1−3). Hydrogen bonding (4−6), van der Waals forces (7), covalent bonding (8−10) and electrostatic interactions (11, 12) have been used to construct multilayer thin films via layer-by-layer assembly. The robust method of electrostatic layer-by-layer (ELBL) assembly typically involves two or more sets of anionically and cationically charged components in combination with a charged substrate or surface of interest. The electrostatic association and binding of oppositely charged components to the substrate permits a simple, low-cost, and versatile method to fabricate thin, well-defined films (13). By these means, the controlled fabrication of multilayer thin films composed of polyelectrolytes (14−17), DNA (18−20), proteins (21, 22), viruses (23), conducting polymers (15, 24−26), and nanoparticles (27−31) has recently been demonstrated. Multilayer thin films formed by incorporating quantum confined nanoparticles have been applied to organic light emitting diodes (15), fuel cell membrane electrodes (32), fast energy transfer nanocrystal bilayers (33−36), thin film diodes (37), donor−acceptor tunnelling layers (38), chemical and biological sensors (39−43), memory elements (44, 45), photodetectors (46), and photovoltaics (47, 48).

In thin film optoelectronics, device architecture is critical to performance (49, 50). It is beneficial if the thin film fabrication method is simple with precise control of thickness, while maximizing interfacial area between material components (51, 52). In ELBL assembly, film deposition is easily controlled by varying the number of iterations in the sequential deposition of anionic and cationic components (1). The two codeposited materials have an inherently high interfacial area because of the repeated and stepwise deposition of nanometer scaled layers of each component. The resulting multilayer film is stabilized by the strong association between oppositely charged components within neighboring layers. Conceptually, ELBL is therefore an excellent synthetic approach to making robust multilayer assemblies with high interfacial area between oppositely charged inorganic semiconductor nanostructures and conjugated polymers.

To demonstrate the fabrication of an inorganic semiconductor/conjugated polymer multilayer for optoelectronics using ELBL assembly, ionically and oppositely charged polythiophenes and CdSe nanoparticles were selected. In the field of thin film photovoltaics for instance, films of intermixed inorganic semiconductors and conjugated polymers have been investigated as photoactive materials in next-generation solar cells (53−60). The photovoltaic activity of the anionically charged polythiophenes, sodium poly[2-(3-thienyl)-ethoxy-4-butylsulfonate] (PTEBS) and poly[3-(potassium-6-hexanoate)thiophene (P3KHT), has recently been

* To whom correspondence should be addressed. E-mail: mbrett@ualberta.ca (M.J.B); jburiak@ualberta.ca (J.M.B).
Received for review September 30, 2009 and accepted December 2, 2009
† Department of Chemistry, University of Alberta.
§ Department of Electrical and Computer Engineering, University of Alberta.
‡ National Institute for Nanotechnology, National Research Council Canada.
DOI: 10.1021/am900659v

established (61−65), and these polythiophenes are promising candidates as material components in ELBL assembled films. In addition, CdSe nanorods (NRs) are a favorable structure in optoelectronics because they provide a pathway for the transport of charge (53). To date however, the synthesis of ionically charged CdSe NRs has not been well-established with few examples in the literature (66, 67). To the authors' knowledge, the ELBL assembly of ionic CdSe NRs and water-soluble polythiophenes has not been demonstrated in the literature. In this work we outline (i) the synthesis of three different aspect ratio CdSe NRs that are dispersible in water, (ii) a thorough characterization of the versatility and nanostructure of ELBL fabricated multilayer thin films of CdSe NRs with PTEBS or P3KHT and (iii) the photovoltaic activity and charge transport of the polythiophene/CdSe NRs multilayer nanocomposite thin films and a thorough analysis on parameters limiting device performance.

## EXPERIMENTAL SECTION

**Materials and General Instrumentation.** Tetradecylphosphonic acid (TDPA) and hexylphosphonic acid (HPA) were used as received from Strem Chemicals Inc.; trioctlyphosphine oxide (TOPO), trioctlyphosphine (TOP), cadmium oxide (CdO), selenium, aminoethanethiol · hydrochloride (AET), high- and low-molecular weight poly(sodium 4-styrenesulfonate) (PSS) ($HM_n$-PSS, $M_n$ = 1 000 000; $LM_n$-PSS, $M_n$ = 70 000), poly(diallyldimethylammonium chloride) (PDDA) ($M_n$ = 400 000−500 000), and 3,4-ethylenedioxythiophene (EDOT) were used as received from Sigma-Aldrich. PTEBS (ADS2000P) was acquired from American Dye Source whereas P3KHT was acquired from Rieke Metals Inc. and both used without further purification. The P3KHT was buffered with phosphate buffer solution (PBS) at a pH of 9. Methanol, ethanol, isopropanol, acetone, toluene, and dichloromethane solvents were used as received from Sigma-Aldrich. Indium tin oxide (ITO) coated glass substrates (8−12 Ω/□) were purchased from Delta Technologies, Ltd. Absorption spectra were recorded on an Agilent UV−vis spectrometer and the solution photoluminescence (PL) was characterized with a PTI (Photon Technology International) fluorescence spectrophotometer. Surfaces were characterized by atomic force microscopy (AFM) using a Nanoscope IV (Digital Instruments/Veeco) instrument, operated in tapping mode with commercially available Si cantilevers (Micromash, freq. = 300 kHz).

**Synthesis of NR1 CdSe Nanorods.** The synthesis of TOPO-capped CdSe NRs follows a modified protocol as outlined in Gur et al. and Wang et al. (68, 69). In brief, 710 mg of tetradecylphosphonic acid (TDPA), 3.00 g of trioctylphosphine oxide (TOPO) and 200 mg of CdO were added to a round-bottom flask and degassed at 120 °C for 30 min under an argon atmosphere. A selenium precursor was made by adding 73 mg of selenium metal to 416 mg of TOP and heating until dissolved. Once dissolved, the mixture was cooled to room temperature. The temperature of the degassing round-bottom flask was then increased to 320 °C to decompose the CdO. The decomposition was accompanied by a transition to a clear and colorless solution. The temperature was further reduced to 280 °C, and the selenium precursor was injected while stirring vigorously. The color of the reaction solution was monitored as it changed from yellow to dark brown indicating increasing aspect ratio nanorods. In the case of NR1, the reaction was stopped when the solution turned red. Once the desired particle length had been reached, the flask was immersed in a water bath to quench the reaction. To purify the nanorods, 3−4 mL of anhydrous toluene was added to the flask. The solution was cleaned using precipitation and centrifugation. The nonsolvent used to precipitate the crystals was methanol. Once added, the mixture was centrifuged for 2 min. The pellets were redispersed in toluene and reprecipitated with methanol. The purification procedure was repeated three times to remove excess TOPO ligand.

**Synthesis of NR2 CdSe Nanorods.** The synthesis of NR2 is analogous to NR1 with the following modifications: 710 mg of tetradecylphosphonic acid (TDPA), 3.00 g of trioctlyphosphine oxide (TOPO), and 80 mg of hexylphosphonic acid (HPA) were used as surfactants. In the case of NR2, the reaction was stopped when the solution turned red.

**Synthesis of NR3 CdSe Nanorods.** The synthesis of NR3 is analogous to NR1 with the following modifications: 710 mg of tetradecylphosphonic acid (TDPA), 3.00 g of trioctlyphosphine oxide (TOPO), and 160 mg of hexylphosphonic acid (HPA) were used as surfactants. Following the trioctylphosphine injection, the temperature was increased to 320 °C followed by the selenium precursor injection. In the case of NR3, the reaction was stopped when the solution turned dark brown.

**AET-CdSe Nanorods.** The ligand exchange process follows a procedure similar to Haremza et al. (70) with minor modifications; 3.2 g of AET was added to a round-bottom flask along with the TOPO-capped nanorods. To this, 20 mL of dichloromethane was added and the solution refluxed at 60 °C overnight under argon in the dark for 12−18 h. At this point, 20 mL of ethanol was added to precipitate the nanorods from the solution and the reflux was continued for an additional hour. To purify the nanorods, the suspension was then centrifuged for 2 min to create AET-CdSe nanorod pellets. The nanorods were then dispersed in methanol with agitation. The purification procedure was repeated six times followed by drying under vacuum. Millipore water was added to the dried pellets, and then the solution was filtered using 0.200 $\mu$m cellulose acetate filters to give optically clear and stable solutions. These solutions were then stored at 4 °C in the dark until use.

**Electrostatic Layer-by-Layer Assembly (ELBL).** The layer-by-layer assembly process was performed using a custom robotic dipper equipped with two Velmex translation axes for lateral and vertical directional movement (see Supporting Information). The entire ELBL apparatus was contained in a box prepurged with nitrogen at a flow rate of 62 sccm for 10 min. The nitrogen flow was maintained for the duration of the run. The temperature within the box was 29 °C. The robotic dipper was kept in the dark for the duration of the film fabrication. Glass, ITO or silicon substrates were cleaned by sequential 10 min ultrasonication in acetone and isopropyl alcohol. Prior to use, the substrates were further cleaned by exposure to 10 min oxygen plasma at ∼0.1 mTorr (Harrick Plasma, PDC 32G, 18W). To generate a single bilayer the following cycle was performed: The negatively charged substrates were immersed in AET-CdSe nanorod solutions that had an optical density of approximately 2.6 for 5 min. The substrate was then removed and rinsed three times using Millipore water (18 MΩ). Following the rinsing, the substrates were then immersed in solutions of polyelectrolyte ($HM_n$-PSS, PTEBS, or P3KHT), at concentrations of 0.5−1 mg/mL, for 5 min, to complete the cycle. These cycles were repeated until the desired number of bilayers was achieved. The pH of all solutions was kept neutral except for P3KHT which was buffered to pH 9 with PBS.

**Photovoltaic Devices.** Devices were fabricated on ITO substrates using the ELBL procedure to generate the photoactive layer. Prior to the ELBL film deposition, polyethylenedioxythiophene:poly(styrenesulfonate) (ePEDOT:PSS) was electrochemically grown from EDOT and $LM_n$-PSS on the ITO at a thickness of approximately 20−30 nm according to literature procedures (71). Onto the active layer, 200 nm of Al was deposited by thermal evaporation at a rate of 10 ± 1 Å/s under high vacuum conditions ($5 \times 10^{-4}$ Pa base pressure, $2 \times 10^{-3}$

Scheme 1. ELBL Process for Forming Nanocomposite Thin Films using CdSe Nanorods, Photoconductive Polymers, and a Variety of Negatively Charged Surfaces[a]

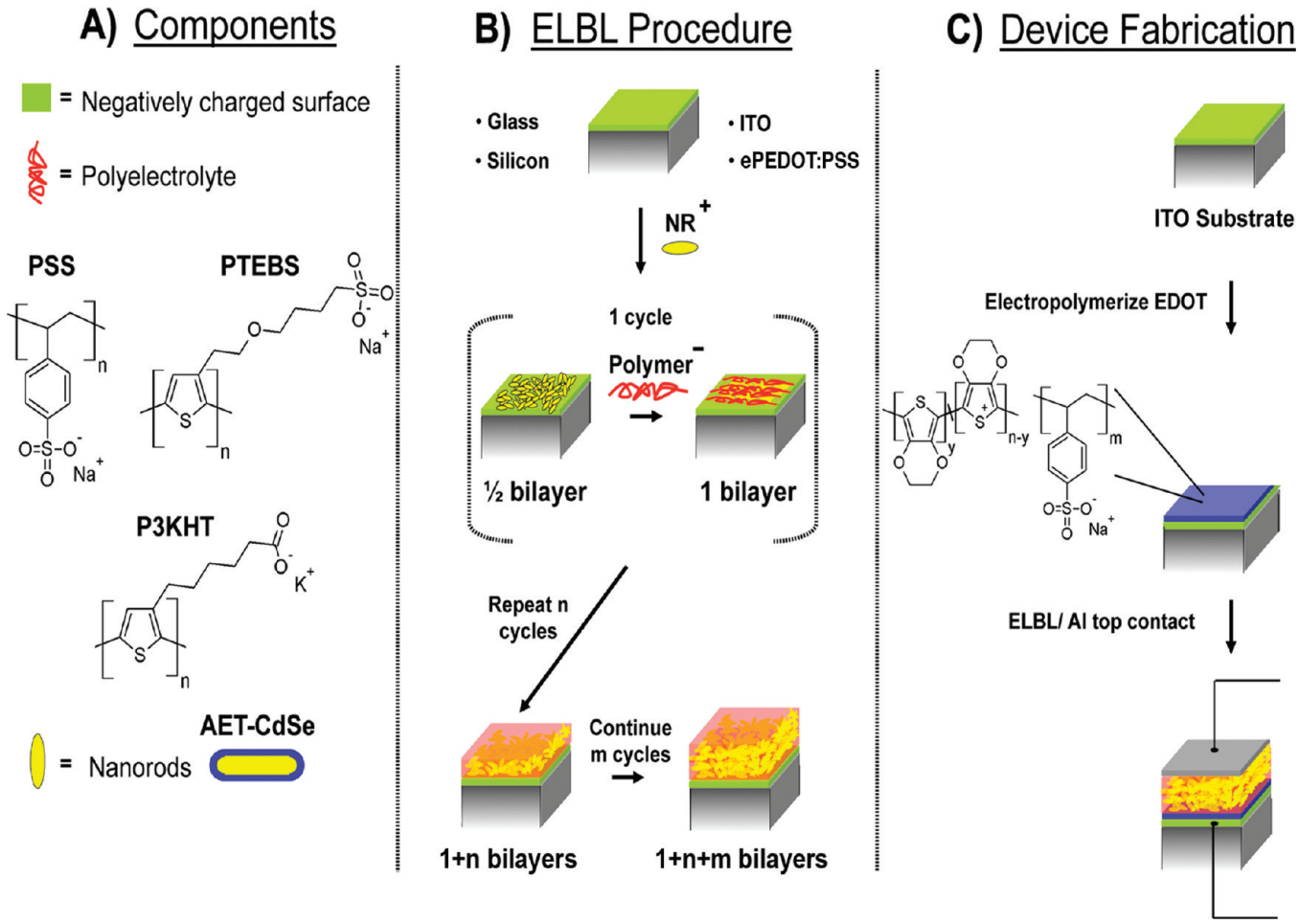


[a] The components, ELBL procedure, and device fabrication are shown in A–C, respectively.

Pa deposition pressure) to complete the device (Scheme 1C). Photovoltaic device testing was performed at ambient atmosphere and temperature under simulated AM 1.5G irradiation using a xenon-lamp-based solar simulator (Oriel 91191 1000W Solar Simulator), with a nominal device irradiation of 100 mW/cm$^2$. The actual irradiance at our test position used for all experiments was calibrated using an NREL-calibrated reference cell of known efficiency (12% efficiency at 25 °C) and found to be 95 mW/cm$^2$. Device characterization was performed using a computer-controlled Keithley 2400 source meter. Fabricated devices were held at a negative bias without illumination to "burn out" short circuit contacts between the ITO anode and Al cathode, and get the devices to exhibit rectifying behavior. The total energy dispersed during the burn out ranged from sub-millijoule to a significant fraction of a joule. Series and shunt resistance were determined by fitting a linear function to the illuminated current density–voltage curves over regions of forward and reverse bias, respectively.

**SEM Cross-Sectioned Samples.** ELBL films deposited on glass or ITO were cleaved with the assistance of a carbide blade and were affixed to SEM mounts with carbon tape. Thin films deposited on glass were sputter-coated with 50 Å of chromium. A Hitachi FE S-4800 SEM was used to image all samples with an accelerating voltage of 10 KV.

**TEM.** Dilute solutions of AET-CdSe nanorods were drop-cast on to 200 mesh copper grids and allowed to dry. A JEOL JEM 2100 TEM with an accelerating voltage of 200 kV was used to image the NRs.

**TEM Cross-Sectioned Samples.** Completed devices were embedded in epoxy (Spurs resin) and cured at (70 °C for 8 h). The solid product was then cracked by sequential dipping in liquid nitrogen and water to remove the glass substrate from the film. This film was then sliced into thin cross-sections using a microtome equipped with a diamond blade. The sliced cross-sections were floated onto carbon-coated copper TEM grids and analyzed using a JEOL JEM 2100 TEM at an accelerating voltage of 200 kV.

**Scanning Auger.** Scanning Auger samples were prepared on a cleaned (ultrasonication with acetone and IPA) silicon substrate using the ELBL procedure. Samples were kept in nitrogen atmosphere until testing. Samples were run on a JAMP 9500F (JEOL) Auger Microscope.

**Cyclic Voltammetry.** Cyclic voltammetry was carried out using a Princeton Applied Research Model 2273 potentiostat employing a standard three-electrode electrochemical cell. All potentials are reported relative to a Ag/Ag$^+$ reference electrode recorded at a scan rate of 50 mV/s. Experiments were carried out at room temperature in acetonitrile containing 0.1 mol L$^{-1}$ tetra(*n*-butyl)ammonium hexafluorophosphate ($^n$Bu$_4$NPF$_6$) as the supporting electrolyte. The counterelectrode was platinum, and the working electrode consisted of a platinum disk (0.071 cm$^2$) coated with a dried film of the material of interest.

**Solution Photoluminescence.** Solution PL was performed with a PTI (Photon Technology International) fluorescence spectrophotometer. Excitation was performed at 500 nm using a Xe lamp at 75 W power. Samples were prepared such that

Scheme 2. Synthetic Method for Producing Nanorods with a Variety of Dimensions[a]

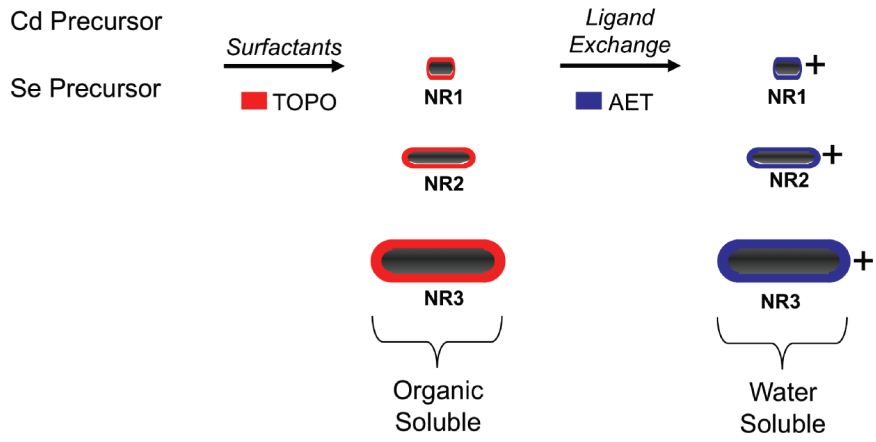


[a] Ligand exchange replaces the organic soluble TOPO for water-soluble AET.

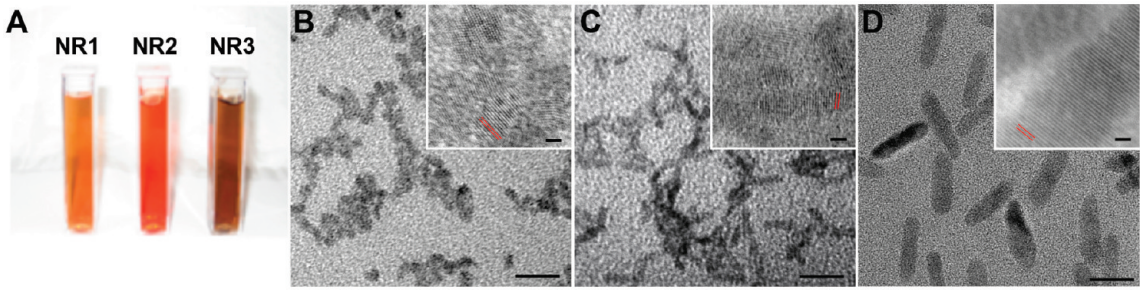


**FIGURE 1. (A) Three AET-capped nanorod solutions made in this study and the TEM micrographs for sample (B) NR1, (C) NR2, and (D) NR3. Insets show HR-TEM images of the three samples with red lines indicating lattice planes (the distance between NR lattice planes in B-D are 0.35 nm, 0.36 and 0.45 nm, respectively). The scale bars in B–D are 20 nm, whereas those in the insets are 2 nm.**

the PTEBS and P3KHT concentrations were held at 1.0 and 0.5 mg/mL respectively, while the CdSe quantum dots were loaded with progressively higher concentrations. The spectra were obtained immediately following the loading of the CdSe.

**Thin Film Photoluminescence.** A series of thin films were constructed on ITO using ELBL assembly including: $(PDDA/PTEBS)_6$, $(PDDA/P3KHT)_6$, $(CdSe\ NR1/PSS)_6$, $(CdSe\ NR1/PTEBS)_6$, and $(CdSe\ NR1/P3KHT)_6$. Solid-state photoluminescence spectroscopy was performed at room temperature, excited at 325 nm from a He–Cd laser. Reflectance was detected using a USB2000 Ocean Optics charge coupled detector (range 300–1050 nm). The spectral response was normalized with a standard blackbody radiator with the blank ITO response subtracted from all spectra with an integration time of 500 ms.

## RESULTS AND DISCUSSION

**Water-Soluble CdSe Nanorods.** Two methods for creating water-soluble nanoparticles are commonly used. The first involves the synthesis of the nanoparticles in water with hydrophilic ligands (72–75), but the synthesis of shapes other than spherical dots remains a challenge for this type of procedure with few known examples (74). The second involves the standard colloidal synthesis of a variety of nanoparticle morphologies in coordinating organic solvents (76–79), followed by substitution of hydrophobic for hydrophilic ligands at the nanoparticle surface to confer water-solubility (66, 67, 70, 75). Using this second method, as outlined in Scheme 2, we synthesized three organic soluble TOPO-capped CdSe NRs by a modified literature procedure and, subsequently, replaced the TOPO ligand with water-soluble AET (68, 69). AET is a short chain ligand that has been used in devices requiring charge transfer (80). Shown in Figure 1A is an optical image of the AET-capped, water-soluble series of CdSe NRs used in this study. All NR solutions were found to be optically clear and stable to precipitation for periods of up to a month.

To investigate the size, morphology, and optical/electrical properties of the AET-stabilized CdSe NRs, TEM, UV–vis, and PL spectroscopy were performed. The NRs were cast from solution (Figure 1A) onto transmission electron microscopy (TEM) grids and the nanorods are shown in Figure 1B–D. The average length by diameter dimensions for NR1, NR2 and NR3 are 5.5 × 4.3, 12.5 × 3.5, and 31.0 × 7.3 nm, respectively, giving the three aspect ratios of 1.3, 3.6, and 4.2. It can be seen from the high resolution TEM (HR-TEM) (Figure 1B–D, insets) that well-defined atomic planes for wurtzite CdSe are present. The optical properties of the water-soluble CdSe NRs were investigated by UV–vis and PL spectroscopy and are presented in Figure 2. A distinct excitonic peak was present in all absorption spectra, and the PL peaks were red-shifted with respect to the absorption (81).

Since these materials were intended for optoelectronic applications, determination of their electronic structure is required. To determine the band gaps, as well as valence and conduction band edges of the nanorods, cyclic voltammetry was utilized (82, 83). As shown in Figure 3, NR1–NR3 were found to have energy gaps that correspond to the gaps

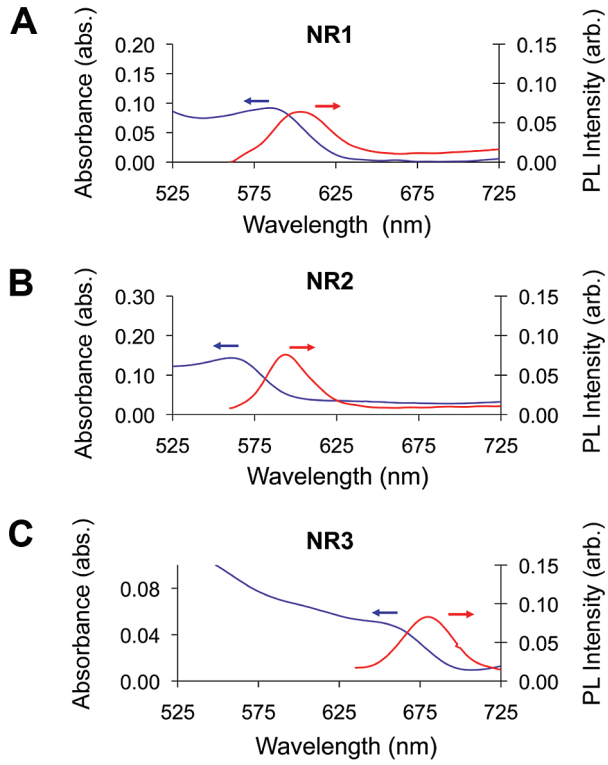


**FIGURE 2. UV−vis and PL spectra for aqueous NR1, NR2, and NR3 (A−C, respectively). Excitation wavelength for emission spectra was 550 nm for NR1, 545 nm for NR2, and 620 nm for NR3.**

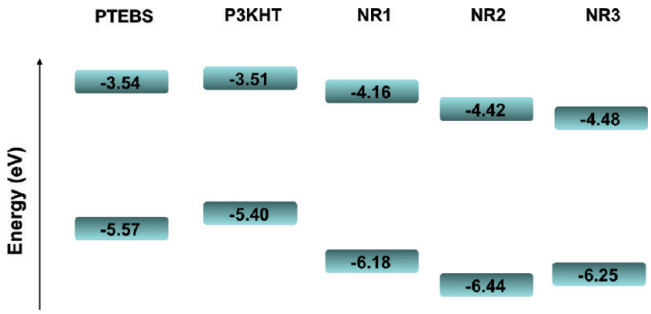


**FIGURE 3. Electronic band edge structure of the three nanorods and two photoconducting polymers as determined by cyclic voltammetry. Values correspond to the energies in electron volts.**

seen in the UV−vis (see Supporting Information). All nanorod samples gave conduction band edge values between −4.16 and −4.48 eV, while the valence band edges are between −6.16 and −6.25 eV. In addition, the highest occupied and lowest unoccupied molecular orbitals (HOMO and LUMO) of the two photoactive polymers used in this study, PTEBS and P3KHT, were investigated using cyclic voltammetry and were included in Figure 3 for comparison.

**Electrostatic Layer-by-Layer Assembly of CdSe Nanorods with PSS, PTEBS, and P3KHT Polyelectrolytes.** The AET-capped nanorods bear amine residues and in water were positively charged. Pairing these nanorods with negatively charged polymers allows one to incorporate them into ELBL multilayer thin films (Scheme 1). Starting with a substrate that has a charged surface, layer-by-layer growth is accomplished by alternating exposure to cationic nanorods and anionic polymers, thus leading to films of controlled thickness and composition. Three anionic polymers were used and include poly(sodium 4-styrenesulfonate) (PSS), a well-established component in various LBL motifs (1, 84, 85), PTEBS and P3KHT, two polythiophenes bearing sulfonate and carboxylate residues, respectively. Figure 4A depicts the optical characterization of the successive bilayer build-up on a glass substrate for PSS and CdSe NR2 components. With increasing bilayer number $n$, there is a corresponding increase in the optical density of the film. The characteristic excitonic peak of the embedded NRs can be seen at approximately 580 nm, a value that closely matches that found in aqueous solution (see Figure 2B). Using the absorbance at 580 nm as a characteristic feature for assessing the growth of the $(CdSe\ NR2/PSS)_n$ multilayer thin film, a plot of these values versus the bilayer number, $n$, was constructed and is shown in Figure 4D. An increase in the optical density with bilayer number was evidenced as seen in other nanorod/polymer systems (5, 86−89). CdSe NR2 and PTEBS exhibit similar trends with increasing optical density with $n$ (Figure 4B and D). To determine the surface roughness of the multilayers, AFM was performed for PSS and NR2 with 0, 10, 20, 30, and 60 bilayers (Figure 5). As seen in Figure 5F, the roughness increases with bilayer number and levels off at higher n. The increasing roughness with bilayer number suggests that the deviation from linearity in the optical density plots in Figure 4D was caused by increases in surface area. With increasing bilayer number, the surface area of the multilayer increases, which in turn leads to more material being deposited during each cycle. This trend resulted in an increase in the absorbance of the films when high bilayer numbers are targeted. A similar trend was also observed for PTEBS multilayers (Figure 5F and Supporting Information).

In the case of P3KHT, which contains carboxylic acids, the solution needed to be buffered to an alkaline pH, in this example pH 9, to produce quality multilayered films. At less than pH 8, there were problems with polymer precipitation after 24 h in solution, and CdSe NR/P3KHT films were found to delaminate, presumably because of the low ionic charge of the protonated polymer. Given that the $pK_a$ of a carboxylic acid is 4−5 (90), adjustment of the pH value of the solution would result in (i) a higher number of deprotonated polymer side-chains and hence an increase in the overall negative charge on the polymer, as well as (ii) the disruption of hydrogen bonding in the P3KHT which may be the mode for solution phase aggregation and hence precipitation (91, 92). With these experimental conditions the $(CdSe\ NR2/P3KHT)_n$ multilayer could be reproducibly constructed and the analogous optical characterization is depicted in Figure 4. Again, increasing optical density and roughness with bilayer number is observed for this system (Figures 4C and 5F and Supporting Information).

To further characterize the ELBL assembly of CdSe NR2 with PSS, $(CdSe\ NR2/PSS)_n$ multilayers were fabricated on glass and investigated in cross-section using SEM. Shown in Figure 6A-C are the tilted, cross-sectional SEM images of $(CdSe\ NR2/PSS)_n$ films, where $n = 10$, 30, and 60, respectively. Inspection of these images indicates that the films

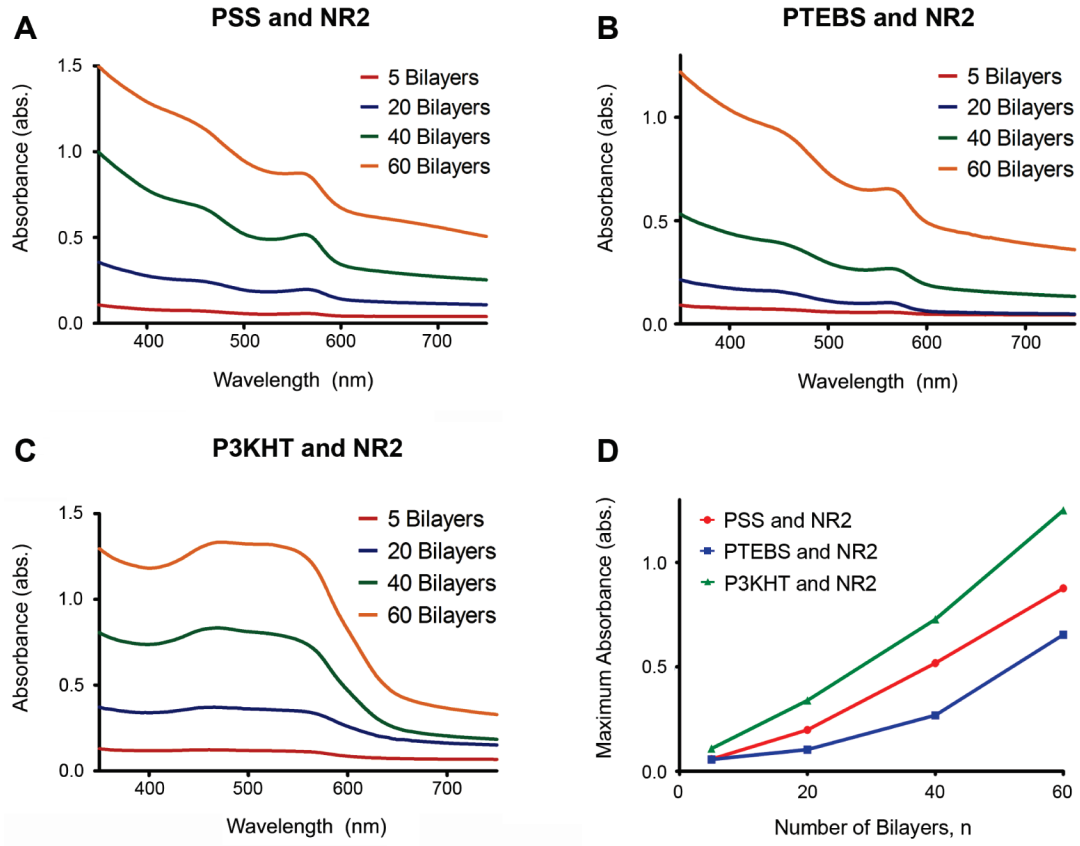


FIGURE 4. Summary of UV−vis experiment monitoring the absorbance of 5, 20, 40, and 60 bilayer films assembled using ELBL on glass with CdSe NR2 (A) PSS, (B) PTEBS, (C) P3KHT, and (D) the summary of the maximum absorbance with increasing bilayer number.

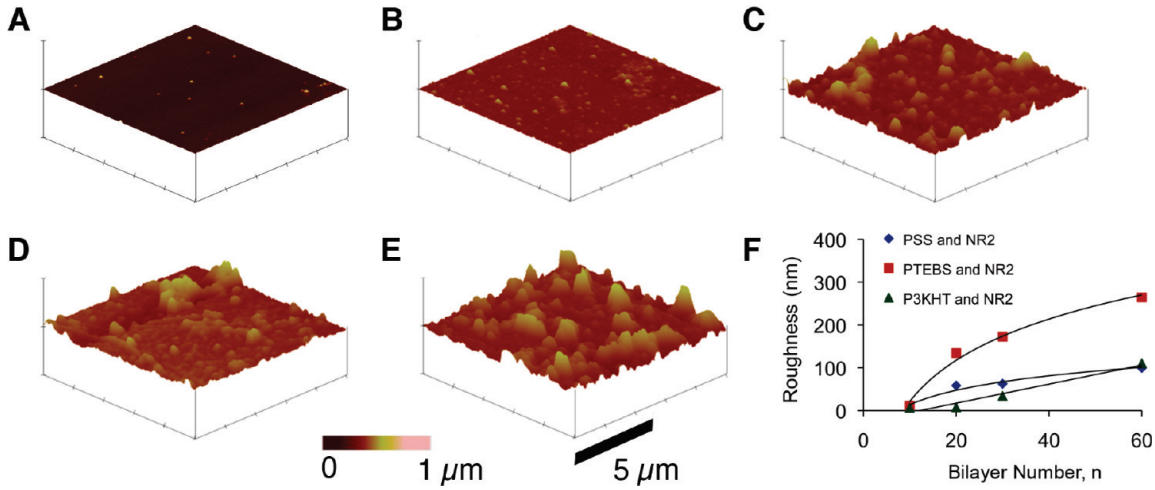


FIGURE 5. AFM study showing the surface of PSS and NR2 films assembled on glass using ELBL after (A) 0 bilayers, (B) 10 bilayers, (C) 20 bilayers, (D) 30 bilayers, and (E) 60 bilayers and (F) the roughness of films after 10, 20, 30, and 60 bilayers for PSS, PTEBS, and P3KHT and NR2 systems.

constructed within this bilayer number range were continuous with an increase in thickness based on $n$. On the basis of the SEM-determined film thickness values of 33, 80, and 140 nm for $(CdSe\ NR2/PSS)_n$ $n = 10$, 30, and 60, respectively, we estimate that each bilayer is 2−3 nm thick, while the smallest NR dimension, the width, is 3 nm. Discrepancies between average bilayer thickness and nanorod dimensions can be rationalized assuming interpenetrating components; in the cases described here, a bilayer does not correspond to a distinct two-layer system with abrupt interfaces. It should be noted that the ELBL films have fairly high rms roughness values and thus all bilayer thicknesses reported in this work represent an average.

Since ELBL assembly with CdSe nanorods and polyelectrolyte has been demonstrated, the process was extended to substrates and polymers that have technological relevance to optoelectronic applications. PEDOT:PSS coated ITO, a commonly used transparent conducting electrode, also successfully functions as a platform onto which ELBL assembly can be performed. PEDOT:PSS is a polymer blend of cationic

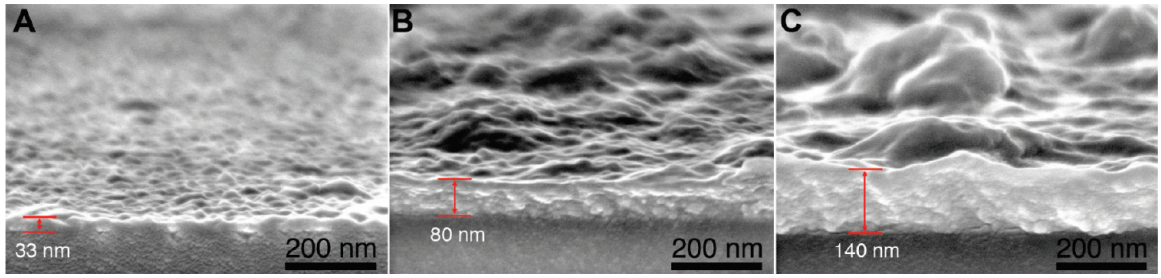


FIGURE 6. SEM cross-sections of $(CdSe\ NR2/PSS)_n$ (A–C, $n = 10, 30, 60$) multilayer nanocomposite thin films on glass.

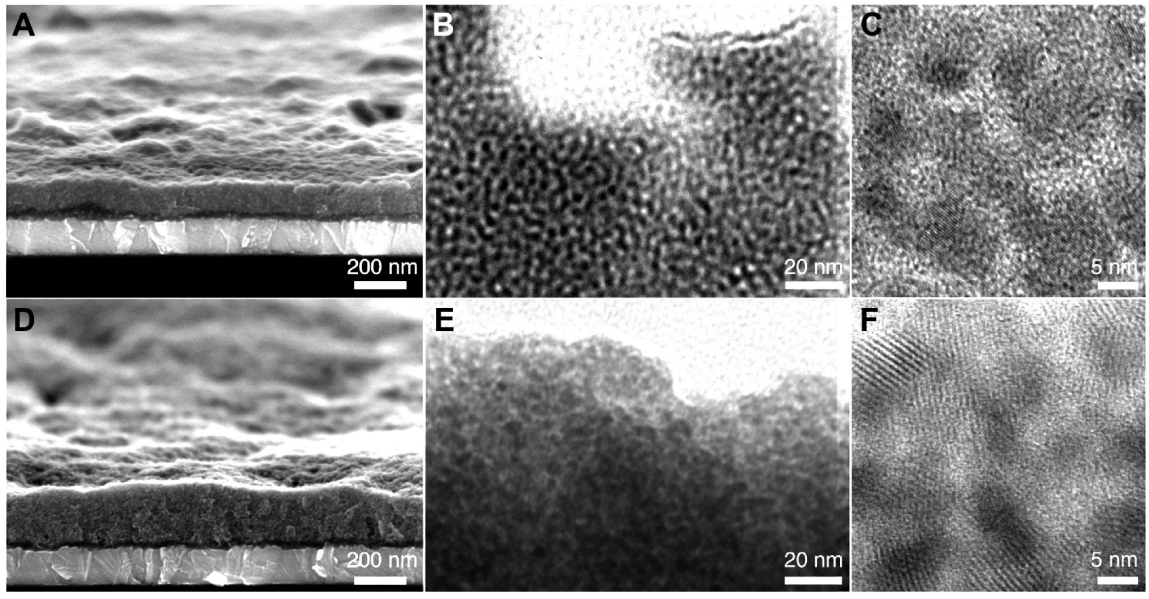


FIGURE 7. Cross-section SEM images of (A) $(CdSe\ NR1/PTEBS)_{60}$ and (D) $(CdSe\ NR2/PTEBS)_{60}$ nanocomposite films (assembled on ITO/ePEDOT:PSS substrate). TEM and HR-TEM cross-sectional analysis of NR1/PTEBS (B and C) and NR2/PTEBS (E and F) nanocomposite films. C and F show the crystal planes of NR1 (0.36 nm) and the moiré fringes of NR2 (0.86 nm).

and conducting PEDOT that is charge-balanced by anionic and insulating PSS. PEDOT:PSS is rich in the PSS component and therefore has an overall negative charge. This material has been widely employed as a hole-collecting interfacial layer at the ITO surface due to its stable and high work function and electron-blocking properties (93). Conventional PEDOT:PSS films were typically applied to ITO using spin-coating techniques, and were found to dissolve during the aqueous ELBL soak; therefore, an alternative coating approach is required. Electrochemically prepared PEDOT:PSS (termed ePEDOT/PSS) has been recently shown to provide a water-insoluble, yet functional, replacement for conventional spin-coated films (71).

Using ePEDOT:PSS-coated ITO, continuous ELBL multilayer films were fabricated from CdSe nanorods and PTEBS polymer, and are shown in Figure 7. $(CdSe\ NR1/PTEBS)_{60}$ and $(CdSe\ NR2/PTEBS)_{60}$ films are 180 and 250 nm thick, respectively, as seen in the tilted SEM cross-sections in Figure 7A and D. In both cases, the ePEDOT:PSS was 30 nm and was grown on 175 nm thick ITO on glass. Following the embedding of these films in epoxy and subsequent sectioning, TEM and HR-TEM images were acquired. The images in Figure 7B and E show the CdSe NRs as darker domains embedded in the PTEBS matrix. The HR-TEM micrographs of the $(CdSe\ NR1/PTEBS)_{60}$ and $(CdSe\ NR2/PTEBS)_{60}$ multilayer films are depicted in Figure 7C and F, respectively. Upon close inspection the lattice planes of the NRs can be seen in Figure 7C, while moiré fringes (94) are present in Figure 7F. Both confirm the presence of nanocrystalline CdSe throughout the bulk of the film. Furthermore, NRs were generally within 5 nm of one another. For further confirmation of the intimate mixing of the NRs and photoactive polymer, a $(CdSe\ NR2/PTEBS)_{60}$ film was fabricated on silicon and analyzed by scanning Auger microscopy (Figure 8). Elemental mapping in the cross-section shows coincident and consistent levels of C, S, Cd, and Se in the film. TEM data in combination with the Auger elemental mapping together point to an intermixed bulk heterojunction (51, 95, 96) of PTEBS and CdSe NRs.

**Photovoltaic Devices Fabricated using ELBL with CdSe Nanorods and Conducting Polymer.** The electrochemical and optical characterization of the photoactive polythiophenes PTEBS and P3KHT suggest that multilayers of these materials in combination with the NRs may exhibit photovoltaic properties (Figure 3). The electrostatically stabilized and intermixed morphology between the donor polythiophenes and the acceptor CdSe NRs in combination with the offset in the band structure suggests a type-II bulk heterojunction may be possible (97) that could result in charge transfer. Photovoltaic (PV) devices were fabricated using a general device architecture of ITO/ePEDOT:PSS/

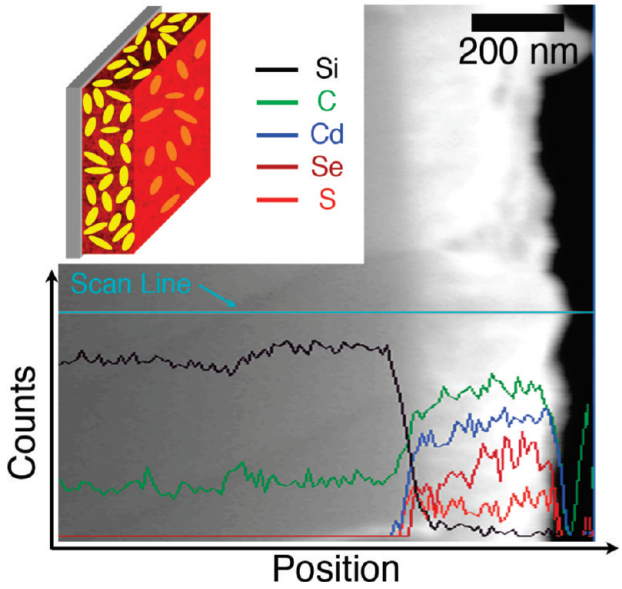


**FIGURE 8. Auger profile scan of (CdSe NR2/PTEBS)$_{60}$ nanorod thin film on silicon. Si, C, Cd, Se, and S line scans are shown as black, green, blue, brown, and red, respectively. The inset illustrates the sample schematic in the orientation of the Auger scan.**

(CdSe NR/polythiophene)$_{60}$/Al (see Scheme 1C) by thermally evaporating Al cathodes directly onto (CdSe NR/polythiophene)$_{60}$ multilayers grown on ITO/ePEDOT:PSS as described earlier. A bilayer number of 60 was chosen as the resulting multilayer films were in the vicinity of the near-optimized 200 nm thickness found by Huynh et al. (55). We have therefore investigated the following multilayers: (CdSe NR1/PTEBS)$_{60}$, (CdSe NR2/PTEBS)$_{60}$, (CdSe NR3/PTEBS)$_{60}$, (CdSe NR1/P3KHT)$_{60}$, and (CdSe NR2/P3KHT)$_{60}$. Figure 9 shows representative cross-sectional SEMs of (CdSe NR1/PTEBS)$_{60}$, (CdSe NR2/PTEBS)$_{60}$, and (CdSe NR3/PTEBS)$_{60}$ multilayer devices. The top Al and bottom ITO contacts can

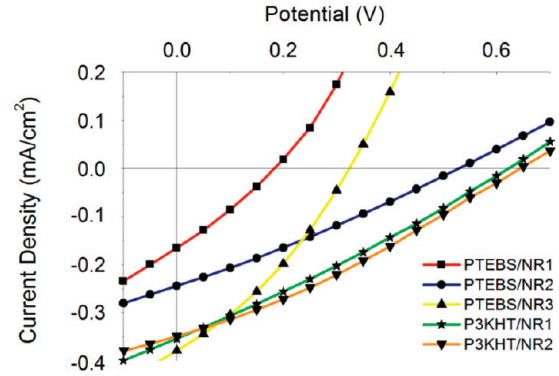


**FIGURE 10. $J-V$ characteristics of the illuminated (CdSe NRx/polymer)$_{60}$ devices made in this study ($x = 1, 2, 3$).**

be seen along with a thin layer of interfacial modifier, ePEDOT:PSS (black), in addition to the multilayered films (textured layer). A higher magnification image of the (CdSe NR3/PTEBS)$_{60}$ device architecture is also presented in Figure 9D. The nanorods were dispersed throughout the bulk of the film. The cross-section SEM images of completed devices further complement the TEM and scanning Auger chemical mapping studies and support a multilayer architecture consisting of highly intermixed components with very high interfacial area.

Figure 10 and Table 1 show and report the current density−voltage ($J-V$) curves and corresponding PV parameters for the 5 types of devices under AM 1.5 simulated solar irradiance. The (CdSe/polythiophene)$_{60}$ multilayers exhibit low power conversion efficiencies of up to 0.07%. Additional statistical data is found in the Supporting Information showing scatter in device performance as the fabrication process is not yet optimized for PV devices. When PTEBS was replaced with P3KHT, a small improvement in device performance was found. It may be that the higher absorbance

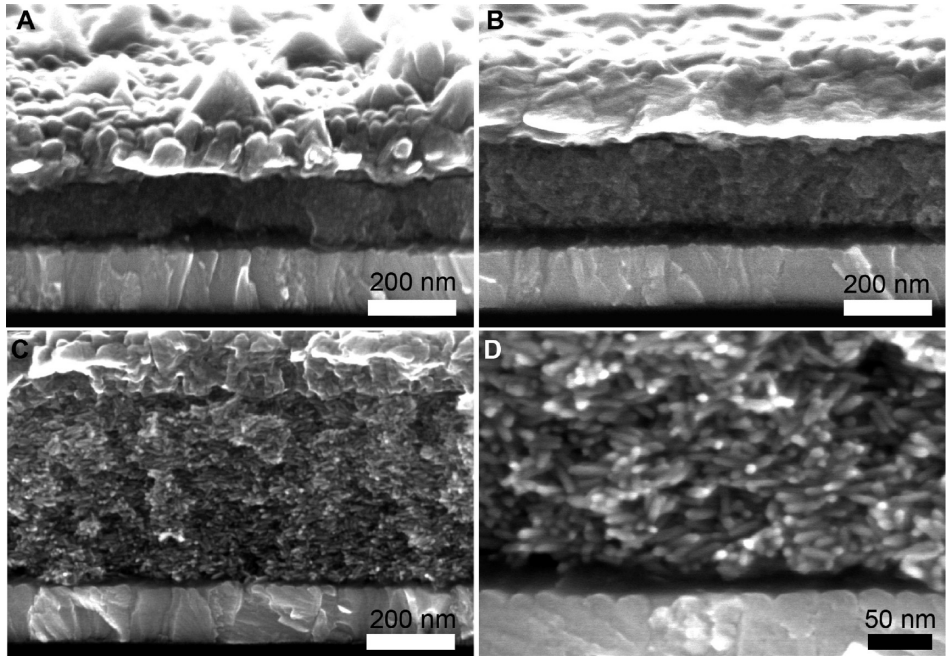


**FIGURE 9. Cross-section SEM of (A) (CdSe NR1/PTEBS)$_{60}$ (B) CdSe NR2/PTEBS)$_{60}$ and (C) CdSe NR3/PTEBS)$_{60}$ completed device architecture using the ELBL technique. A high magnification SEM of the film in (C) is shown in (D).**

**Table 1. PV Characteristics of the Best Performing Examples of ELBL-Assembled Solar Cells Made in This Study Showing the Nanorod Aspect Ratio (AR), Power Conversion Efficiency ($\eta$), Open Circuit Potential ($V_{OC}$), Fill Factor (FF), and Short Circuit Current ($J_{SC}$)[a]**

| | Material | AR | $J_{sc}$ (mA/cm$^2$) | $V_{oc}$ (V) | *FF* | $\eta$ (%) |
|---|---|---|---|---|---|---|
| PTEBS | NR1 | 1.3 | -0.17 | 0.18 | 0.29 | 0.010 |
| | NR2 | 3.6 | -0.23 | 0.44 | 0.28 | 0.030 |
| | NR3 | 4.2 | -0.38 | 0.32 | 0.32 | 0.042 |
| P3KHT | NR1 | 1.3 | -0.35 | 0.62 | 0.28 | 0.064 |
| | NR2 | 3.6 | -0.35 | 0.65 | 0.30 | 0.071 |

[a] Data represents the highest efficiency values from 10 regions on two substrates and are representative of the generally observed trend. (Additional statistics shown in Supporting Information).

cross-section of the (CdSe NR1/P3KHT)$_{60}$ and (CdSe NR2/P3KHT)$_{60}$ multilayer films (refer to Figure 4C) lead to a higher number of absorbed photons and a commensurate accumulation of excitons in these films.

**Analysis of ELBL PV Devices.** Although the devices show some photoactive response, their performance is relatively poor. To investigate the factors leading to the lack of photoactivity, a thorough analysis of the power conversion process was conducted. Two critical parameters governing device performance include the short circuit current ($J_{sc}$) and open circuit voltage ($V_{oc}$) extracted from the $J-V$ curves. In general, the $V_{oc}$ values of the devices compare to similar literature systems (10, 54−59) suggesting that the $J_{sc}$ is the limiting factor affecting the device performance.

A high short circuit current in optoelectronic thin films requires the following: absorption of photons to generate excitons, exciton diffusion, charge transfer and carrier transport. From Figure 4, the ELBL assembled films demonstrate good absorption cross-sections covering a large portion of the visible region. In addition, the characteristic domain sizes of NR and polythiophene phases are on the order of the exciton diffusion length (Figure 7) (98−100). To probe the charge transfer in the films, solution and thin film photoluminescence (PL) quenching experiments were performed. The PTEBS and P3KHT solution PL spectra are shown in Figure 11. As can be seen from Figure 3, the driving force for electron transfer ($\Delta E$ = LUMO$_{donor}$ − LUMO$_{acceptor}$) from the two polythiophenes to the NR series is expected to be the lowest for NR1. For this reason, we chose to investigate the NR1/polymer system, since evidence for charge transfer in this least favored system strongly suggests the possibility for charge transfer in the NR2 and NR3 systems, which have more suitable energy levels. When increasing amounts of CdSe NR1 were added to the PTEBS and P3KHT solutions, the PL signal diminished in intensity, which suggests effective charge transfer from the donor polymer to the acceptor, CdSe NR1. To further investigate charge transfer, solid-state PL spectroscopy was performed on (CdSe NR1/PTEBS)$_6$ and (CdSe NR1/P3KHT)$_6$ ELBL assembled films. Thiophene-only films were electrostatically assembled using poly(diallyldimethylammonium chloride) (PDDA) as the cationic component while CdSe NR-only films were assembled with PSS anions. The PL spectra of the (CdSe NR1/PTEBS)$_6$ system is illustrated in Figure 11C. The PL signals for the CdSe- and PTEBS-only films are clearly seen while the combined (CdSe NR1/PTEBS)$_6$ films have very little PL signal. This strongly suggests electron transfer from PTEBS to CdSe in ELBL assembled thin films. A similar quenching of the PL signal is observed for the (CdSe NR1/P3KHT)$_6$ system as seen in Figure 11D.

Since exciton formation and dissociation appear to be achieved, carrier transport is likely the source of the low $J_{sc}$

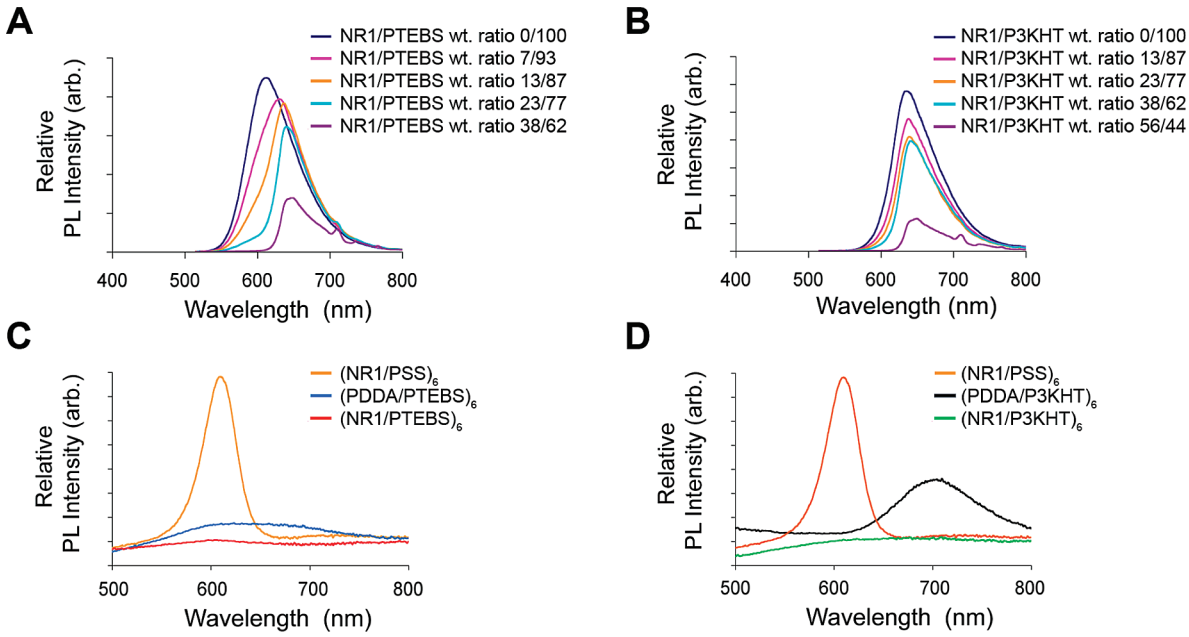


**FIGURE 11. Photoluminescence spectra of (A) PTEBS solutions with increasing CdSe NR1 content, (B) P3KHT solutions with increasing CdSe NR1 content, (C) ELBL films of (CdSe NR1/PSS)$_6$, (PDDA/PTEBS)$_6$ and (PTEBS/CdSe NR1)$_6$ composite, and (D) films of (CdSe NR1/PSS)$_6$, (PDDA/P3KHT)$_6$, and (P3KHT/CdSe NR1)$_6$ composite.**

values and thus the poor photovoltaic performance. To elucidate this point, the series and shunt resistances were estimated from the slopes of the $J-V$ curves in the heavily forward biased and reverse biased regions respectively. Table 2 in the Supporting Information lists the series and shunt resistances of our devices. From the AFM analysis in Figure 5, it can be seen that the ELBL films have very high rms roughness, particularly the NR/PTEBS composites that gave poorer performing devices. This likely contributes to the low shunt resistances. Much more pronounced are the large series resistance values. Factors influencing the series resistance include nanorod−nanorod contact, nanorod orientation, and surface ligands; all of which affect carrier transport. From the analysis in Figure 7, we may conclude that although many of the nanorods lie in close proximity to one another, they may not be in direct (i.e., ohmic) contact because of the presence of interstitial polymer. As a result, a large number of interparticle hopping events are required throughout the film subsequent to charge transfer. From the SEM image in Figure 9D, it can be seen that most nanorods lie parallel to the electrode surface as opposed to the ideal vertical alignment. The above analysis thus suggests that further optimization is required to increase the $J_{SC}$ and improve device performance.

The investigations into the utility of the (CdSe/polythiophene)$_{60}$ multilayer films are preliminary and we anticipate that lengthy and thorough optimization, including annealing procedures, introduction of charge blocking interfaces, substitution of nanorod ligands, multilayer thicknesses and other photoactive polymers, may lead to improved PV performance, and this is currently the focus of our efforts.

## CONCLUSION

In summary, a facile and versatile all-aqueous method for fabricating CdSe nanorod/polymer nanocomposite thin films was reported. Using ligand-exchange chemistry, water-soluble nanorods of varying length and properties were synthesized. The water-soluble cationic nanorods and anionic polymers were incorporated into multilayer thin films with controlled thicknesses using electrostatic layer-by-layer assembly (ELBL). The presence of a polymer/nanorod bulk heterojunction was shown with cross-sectional SEM, TEM, and scanning Auger analysis. Optoelectronic devices were fabricated by employing ELBL on transparent conducting electrodes. Although devices had low conversion efficiencies, performance analysis of the $J-V$ curves in combination with multilayer PL spectroscopy suggests carrier transport is the primary factor limiting photovoltaic properties.

**Acknowledgment.** This work was supported by the Natural Sciences and Engineering Research Council of Canada (NSERC), NRC-NINT, the University of Alberta, Micralyne Inc, iCORE, the Canadian Foundation for Innovation and Alberta Ingenuity Fund (J.A.M.F.). D.A.R. and M.F. acknowledge the Killam Foundation for PDF fellowships. Dr. Sun at the Cross Cancer Institute and Dr. Chen in the Department of Medicine and Dentistry at the University of Alberta are thanked for their assistance with TEM. Abeed Lalany is acknowledged for Al Deposition and PV device testing, as well as Dr. Michael Taschuk for extensive work in calibrating the solar simulator. Dr. Al Meldrum and Ross Lockwood are thanked for access to and assistance with PL spectroscopy.

**Supporting Information Available:** Figures and tables with eLBL apparatus, further characterization of the polymers and CdSe NRs, statistical data on photovoltaic characteristics, light and dark curves for all devices, additional device cross-sections, AFM illustrating surface roughness trends and calculated series and shunt resistances. This information is available free of charge via the Internet at http://pubs.acs.org.

## REFERENCES AND NOTES

(1) Decher, G. *Science* **1997**, *277* (5330), 1232–1237.
(2) Caruso, F. *Adv. Mater.* **2001**, *13* (1), 11–12.
(3) Schreiber, F. *Prog. Surf. Sci.* **2000**, *65* (5−8), 151–256.
(4) Hammond, P. T. *Adv. Mater.* **2004**, *16* (15), 1271–1293.
(5) Hao, E. C.; Lian, T. Q. *Langmuir* **2000**, *16* (21), 7879–7881.
(6) De Girolamo, J.; Reiss, P.; Pron, A. *J. Phys. Chem. C* **2008**, *112* (24), 8797–8801.
(7) Sato, M.; Sano, M *Langmuir* **2005**, *21* (24), 11490–11494.
(8) Cui, J.; Huang, Q. L.; Wang, Q. W.; Marks, T. J. *Langmuir* **2001**, *17* (7), 2051–2054.
(9) Tian, Y.; He, Q.; Tao, C.; Li, J. B. *Langmuir* **2006**, *22* (1), 360–362.
(10) Liang, Z. Q.; Dzienis, K. L.; Xu, J.; Wang, Q. *Adv. Funct. Mater.* **2006**, *16* (4), 542–548.
(11) Lvov, Y.; Ariga, K.; Ichinose, I.; Kunitake, T. *J. Am. Chem. Soc.* **1995**, *117* (22), 6117–6123.
(12) Lee, S. H.; Balasubramanian, S.; Kim, D. Y.; Viswanathan, N. K.; Bian, S.; Kumar, J.; Tripathy, S. K. *Macromolecules* **2000**, *33* (17), 6534–6540.
(13) Decher, G.; Schlenoff, J. B. *Multilayer Thin Films: Sequential Assembly of Nanocomposite Materials*, Wiley-VCH: Weinheim, Germany, 2003; p 524.
(14) Wang, X. Y.; Kim, Y. G.; Drew, C.; Ku, B. C.; Kumar, J.; Samuelson, L. A. *Nano Lett.* **2004**, *4* (2), 331–334.
(15) Ho, P. K. H.; Kim, J. S.; Burroughes, J. H.; Becker, H.; Li, S. F. Y.; Brown, T. M.; Cacialli, F.; Friend, R. H. *Nature* **2000**, *404* (6777), 481–484.
(16) Bertrand, P.; Jonas, A.; Laschewsky, A.; Legras, R. *Macromol. Rapid Commun.* **2000**, *21* (7), 319–348.
(17) Shiratori, S. S.; Rubner, M. F. *Macromolecules* **2000**, *33* (11), 4213–4219.
(18) Jordan, C. E.; Frutos, A. G.; Thiel, A. J.; Corn, R. M. *Anal. Chem.* **1997**, *69* (24), 4939–4947.
(19) Pei, R. J.; Cui, X. Q.; Yang, X. R.; Wang, E. K. *Biomacromolecules* **2001**, *2* (2), 463–468.
(20) Johnston, A. P. R.; Read, E. S.; Caruso, F. *Nano Lett.* **2005**, *5* (5), 953–956.
(21) Caruso, F.; Niikura, K.; Furlong, D. N.; Okahata, Y. *Langmuir* **1997**, *13* (13), 3427–3433.
(22) Caruso, F.; Mohwald, H. *J. Am. Chem. Soc.* **1999**, *121* (25), 6039–6046.
(23) Yoo, P. J.; Nam, K. T.; Qi, J. F.; Lee, S. K.; Park, J.; Belcher, A. M.; Hammond, P. T. *Nat. Mater.* **2006**, *5* (3), 234–240.
(24) Mwaura, J. K.; Pinto, M. R.; Witker, D.; Ananthakrishnan, N.; Schanze, K. S.; Reynolds, J. R *Langmuir* **2005**, *21* (22), 10119–10126.
(25) Ramey, M. B.; Hiller, J. A.; Rubner, M. F.; Tan, C. Y.; Schanze, K. S.; Reynolds, J. R. *Macromolecules* **2005**, *38* (2), 234–243.
(26) Pinto, M. R.; Kristal, B. M.; Schanze, K. S. *Langmuir* **2003**, *19* (16), 6523–6533.
(27) Kim, J.; Lee, S. W.; Hammond, P. T.; Shao-Horn, Y. *Chem. Mater.* **2009**, *21* (13), 2993–3001.
(28) Lowman, G. M.; Nelson, S. L.; Graves, S. A.; Strouse, G. F.; Buratto, S. K. *Langmuir* **2004**, *20* (6), 2057–2059.
(29) Zhang, Q.; Atay, T.; Tischler, J. R.; Bradley, M. S.; Bulovic, V.; Nurmikko, A. V. *Nat. Nanotechnol.* **2007**, *2* (9), 555–559.

(30) Kim, H. S.; Sohn, B. H.; Lee, W.; Lee, J. K.; Choi, S. J.; Kwon, S. J. *Thin Solid Films* **2002**, *419* (1−2), 173–177.
(31) Wang, S. B.; Li, C.; Shi, G. Q. *Sol. Energy Mater. Sol. Cells* **2008**, *92* (5), 543–549.
(32) Taylo, A. D.; Michel, M.; Sekol, R. C.; Kizuka, J. M.; Kotov, N. A.; Thompson, L. T. *Adv. Funct. Mater.* **2008**, *18* (19), 3003–3009.
(33) Franzl, T.; Koktysh, D. S.; Klar, T. A.; Rogach, A. L.; Feldmann, J.; Gaponik, N. *Appl. Phys. Lett.* **2004**, *84* (15), 2904–2906.
(34) Franzl, T.; Shavel, A.; Rogach, A. L.; Gaponik, N.; Klar, T. A.; Eychmuller, A.; Feldmann, J *Small* **2005**, *1* (4), 392–395.
(35) Franzl, T.; Klar, T. A.; Schietinger, S.; Rogach, A. L.; Feldmann, J. *Nano Lett.* **2004**, *4* (9), 1599–1603.
(36) Klar, T. A.; Franzl, T.; Rogach, A. L.; Feldmann, J. *Adv. Mater.* **2005**, *17* (6), 769–773.
(37) Cassagneau, T.; Mallouk, T. E.; Fendler, J. H. *J. Am. Chem. Soc.* **1998**, *120* (31), 7848–7859.
(38) Gross, D.; Susha, A. S.; Klar, T. A.; Da Como, E.; Rogach, A. L.; Feldmann, J. *Nano Lett.* **2008**, *8* (5), 1482–1485.
(39) Beissenhirtz, M. K.; Scheller, F. W.; Lisdat, F. *Anal. Chem.* **2004**, *76* (16), 4665–4671.
(40) Slater, J. M.; Paynter, J.; Watt, E. J. *Analyst* **1993**, *118* (4), 379–384.
(41) Decher, G.; Lehr, B.; Lowack, K.; Lvov, Y.; Schmitt, J. *Biosens. Bioelectron.* **1994**, *9* (9−10), 677–684.
(42) Anzai, J.; Takeshita, H.; Kobayashi, Y.; Osa, T.; Hoshi, T. *Anal. Chem.* **1998**, *70* (4), 811–817.
(43) Zheng, L. Z.; Yao, X.; Li, J. H. *Curr. Anal. Chem.* **2006**, *2* (3), 279–296.
(44) Das, B. C.; Batabyal, S. K.; Pal, A. J. *Adv. Mater.* **2007**, *19* (23), 4172–4176.
(45) Sahu, S.; Majee, S. K.; Pal, A. J. *Appl. Phys. Lett.* **2007**, *91*, 14–143108.
(46) Tu, C. C.; Lin, L. Y. *Appl. Phys. Let.* **2008**, *93*, 16–163107.
(47) Masuda, K.; Ogawa, M.; Ohkita, H.; Benten, H.; Ito, S. *Sol. Energy Mater. Sol. Cells* **2009**, *93* (6−7), 762–767.
(48) Kniprath, R.; McLeskey, J. T.; Rabe, J. P.; Kirstein, S. *J. Appl. Phys.* **2009**, *105*, 12–124313.
(49) Peumans, P.; Yakimov, A.; Forrest, S. R. *J. Appl. Phys.* **2003**, *93* (7), 3693–3723.
(50) Coakley, K. M.; McGehee, M. D. *Chem. Mater.* **2004**, *16* (23), 4533–4542.
(51) Saunders, B. R.; Turner, M. L *Adv. Colloid Interface Sci.* **2008**, *138* (1), 1–23.
(52) Sanchez, C.; Julian, B.; Belleville, P.; Popall, M. *J. Mater. Chem.* **2005**, *15* (35−36), 3559–3592.
(53) Oosterhout, S. D.; Wienk, M. M.; van Bavel, S. S.; Thiedmann, R.; Koster, L. J. A.; Gilot, J.; Loos, J.; Schmidt, V.; Janssen, R. A. J. *Nat. Mater.* **2009**, *8* (10), 818–824.
(54) Huynh, W. U.; Dittmer, J. J.; Alivisatos, A. P *Science* **2002**, *295* (5564), 2425–2427.
(55) Huynh, W. U.; Dittmer, J. J.; Libby, W. C.; Whiting, G. L.; Alivisatos, A. P. *Adv. Funct. Mater.* **2003**, *13* (1), 73–79.
(56) Sun, B. Q.; Marx, E.; Greenham, N. C. *Nano Lett.* **2003**, *3* (7), 961–963.
(57) Sun, B. Q.; Greenham, N. C. *Phys. Chem. Chem. Phys.* **2006**, *8* (30), 3557–3560.
(58) Aldakov, D.; Chandezon, F.; De Bettignies, R.; Firon, M.; Reiss, P.; Pron, A. *Eur. Phys. J. Appl. Phys.* **2006**, *36* (3), 261–265.
(59) Olson, J. D.; Gray, G. P.; Carter, S. A. *Sol. Energy Mater. Sol. Cells* **2009**, *93* (4), 519–523.
(60) Guldi, D. M.; Zilberman, I.; Anderson, G.; Kotov, N. A.; Tagmatarchis, N.; Prato, M. *J. Mater. Chem.* **2005**, *15* (1), 114–118.
(61) Qiao, Q. Q.; Xie, Y.; McLeskey, J. T. *J. Phys. Chem. C* **2008**, *112* (26), 9912–9916.
(62) Yang, J. H.; Garcia, A.; Nguyen, T. Q. *Appl. Phys. Lett.* **2007**, *90*, 103514-1−103514-3.
(63) Shankar, K.; Mor, G. K.; Prakasam, H. E.; Varghese, O. K.; Grimes, C. A. *Langmuir* **2007**, *23*, 12445–12449.
(64) Lohwasser, R. H.; Bandara, J.; Thelakkat, M. *J. Mater. Chem.* **2009**, *19* (24), 4126–4130.
(65) Mwaura, J. K.; Zhao, X. Y.; Jiang, H.; Schanze, K. S.; Reynolds, J. R. *Chem. Mater.* **2007**, *19* (5), 1202–1202.
(66) Artemyev, M.; Kisiel, D.; Abmiotko, S.; Antipina, M. N.; Khomutov, G. B.; Kislov, V. V.; Rakhnyanskaya, A. A. *J. Am. Chem. Soc.* **2004**, *126*, 10594–10597.
(67) Sukhanova, A.; Baranov, A. V.; Klinov, D.; Oleinikov, V.; Berwick, K.; Cohen, J. H. M.; Pluot, M.; Nabiev, I. *Nanotechnology* **2006**, *17*, 4223–4228.
(68) Gur, I.; Fromer, N. A.; Geier, M. L.; Alivisatos, A. P *Science* **2005**, *310* (5747), 462–465.
(69) Wang, W.; Banerjee, S.; Jia, S. G.; Steigerwald, M. L.; Herman, I. P. *Chem. Mater.* **2007**, *19* (10), 2573–2580.
(70) Haremza, J. M.; Hahn, M. A.; Krauss, T. D. *Nano Lett.* **2002**, *2* (11), 1253–1258.
(71) Rider, D. A.; Harris, K. D.; Wang, D.; Bruce, J.; Fleischauer, M. D.; Tucker, R. T.; Brett, M. J.; Buriak, J. M. *ACS Appl. Mater. Interfaces* **2009**, *1* (2), 279–288.
(72) Xing, R. M.; Wang, X. Y.; Yan, L. L.; Zhang, C. L.; Yang, Z.; Wang, X. H.; Guo, Z. J. *Dalton Trans.* **2009**, *10*, 1710–1713.
(73) Gaponik, N.; Talapin, D. V.; Rogach, A. L.; Hoppe, K.; Shevchenko, E. V.; Kornowski, A.; Eychmuller, A.; Weller, H. *J. Phys. Chem. B* **2002**, *106* (29), 7177–7185.
(74) Schulz-Drost, C.; Sgobba, V.; Guldi, D. M. *J. Phys. Chem. C* **2007**, *111* (27), 9694–9703.
(75) Fang, Z.; Liu, L.; Xu, L. L.; Yin, X. G.; Zhong, X. H. *Nanotechnology* **2008**, *19* (23), 235603.
(76) Alivisatos, A. P. *Science* **1996**, *271* (5251), 933–937.
(77) Manna, L.; Scher, E. C.; Alivisatos, A. P. *J. Am. Chem. Soc.* **2000**, *122* (51), 12700–12706.
(78) Peng, Z. A.; Peng, X. G. *J. Am. Chem. Soc.* **2001**, *123* (1), 183–184.
(79) Peng, X. G.; Manna, L.; Yang, W. D.; Wickham, J.; Scher, E.; Kadavanich, A.; Alivisatos, A. P. *Nature* **2000**, *404* (6773), 59–61.
(80) Landi, B. J.; Castro, S. L.; Ruf, H. J.; Evans, C. M.; Bailey, S. G.; Raffaelle, R. P. *Sol. Energy Mater. Sol. Cells* **2005**, *87*, 733–746.
(81) Murray, C. B.; Kagan, C. R.; Bawendi, M. G. *Annu. Rev. Mater. Sci.* **2000**, *30*, 545–610.
(82) Inamdar, S. N.; Ingole, P. P.; Haram, S. K. *ChemPhysChem* **2008**, *9* (17), 2574–2579.
(83) Kucur, E.; Riegler, J.; Urban, G. A.; Nann, T. *J. Chem. Phys.* **2003**, *119* (4), 2333–2337.
(84) Decher, G.; Hong, J. D.; Schmitt, J. *Thin Solid Films* **1992**, *210* (1−2), 831–835.
(85) Srivastava, S.; Kotov, N. A. *Acc. Chem. Res.* **2008**, *41* (12), 1831–1841.
(86) Kim, D.; Okahara, S.; Shimura, K.; Nakayama, M. *J. Phys. Chem. C* **2009**, *113* (17), 7015–7018.
(87) Mohanta, K.; Majee, S. K.; Batabyal, S. K.; Pal, A. J *J. Phys Chem. B* **2006**, *110* (37), 18231–18235.
(88) Zhai, L.; McCullough, R. D. *Adv. Mater.* **2002**, *14* (12), 901–905.
(89) Zucolotto, V.; Gattas-Asfura, K. M.; Tumolo, T.; Perinotto, A. C.; Antunes, P. A.; Constantino, C. J. L.; Baptista, M. S.; Leblanc, R. M.; Oliveira, O. N. *Appl. Surf. Sci.* **2005**, *246* (4), 397–402.
(90) Lide, D. R. *CRC Handbook of Chemistry and Physics*; CRC Press LLC: Boca Raton, FL, 2003; Vol. 84.
(91) McCullough, R. D.; Ewbank, P. C.; Loewe, R. S. *J. Am. Chem. Soc.* **1997**, *119* (3), 633–634.
(92) Kim, B. S.; Chen, L.; Gong, J. P.; Osada, Y. *Macromolecules* **1999**, *32* (12), 3964–3969.
(93) Roman, L. S.; Mammo, W.; Pettersson, L. A. A.; Andersson, M. R.; Inganas, O. *Adv. Mater.* **1998**, *10* (10), 774–777.
(94) Reyes-Gasga, J.; Tehuacanero, S.; Yacaman, M. J. *Microsc. Res. Tech.* **1998**, *40* (1), 2–9.
(95) Coakley, K. M.; McGehee, M. D. *Chem. Mater.* **2004**, *16*, 4533–4542.
(96) Blom, P. W. M.; Mihailetchi, V. D.; Koster, L. J. A.; Markov, D. E. *Adv. Mater.* **2007**, *19* (12), 1551–1566.
(97) Franciosi, A.; VandeWalle, C. G. *Surf. Sci. Rep.* **1996**, *25* (1−4), 1–140.
(98) Gregg, B. A. *J. Phys. Chem. B* **2003**, *107* (20), 4688–4698.
(99) Yoo, S.; Potscavage, W. J.; Domercq, B.; Han, S. H.; Li, T. D.; Jones, S. C.; Szoszkiewicz, R.; Levi, D.; Riedo, E.; Marder, S. R.; Kippelen, B. *Solid-State Electron.* **2007**, *51* (10), 1367–1375.
(100) Sgobba, V.; Troeger, A.; Cagnoli, R.; Mateo-Alonso, A.; Prato, M.; Parenti, F.; Mucci, A.; Schenetti, L.; Guldi, D. M. *J. Mater. Chem.* **2009**, *19*, 4319–4324.


AM900659V